Astron. Astrophys. 361, 734–742 (2000)

ASTRONOMY AND ASTROPHYSICS

Spectral signature of uncombed penumbral magnetic fields

V. Martínez Pillet

Instituto de Astrofísica de Canarias, 38200 La Laguna, Tenerife, Spain (vmp@ll.iac.es)

Received 24 January 2000 / Accepted 17 February 2000

Abstract. The uncombed penumbral model proposed by Solanki & Montavon (1993) is used to understand some recent observational results found in penumbrae. This model uses a penumbral magnetic field structured into horizontal flux tubes embedded in a more vertical background field. A modified version of this model, with a weaker field strength in the horizontal tubes, is used to explain the gradient with height of field strength and inclination found in studies using inversion techniques. These studies have found that over a range of 300 km, the field strength of the outer penumbra increases with height by more than 500 G. Similarly, the field inclination decreases with height by 30° in the same range of heights. We show that spectra generated by the uncombed model can give rise to these two effects as long as the horizontal tubes (of ∼100 km diameter) remain unresolved. We also study the linear, quadratic and rms fluctuations of the inclination gradients that can be generated by the uncombed model. These gradients are found to be compatible with those obtained from the null divergence condition and those derived from observations of net circular polarization. A key ingredient to explain these gradients is the contribution of the two boundary layers that enclose the horizontal magnetic tubes as seen by the line-of-sight. Our realization of the uncombed model also predicts values of the net circular polarization observed with the Advanced Stokes Polarimeter. The existence of a pure background penumbral field as proposed by the model is, however, put into question.

Key words: Sun: sunspots – Sun: magnetic fields

1. Introduction

In contrast to the dark umbrae of sunspots, penumbrae have a heat flux that is around 75% that of the normal quiet sun (see, e.g., Schmidt 1991). It is clear that convective motions that are only slightly less efficient than the normal granulation should be responsible for the penumbral brightness. The nature of these convective motions is not yet known. But recent models of interchange convection of magnetic flux tubes look promising (Schlichenmaier et al. 1998, Jahn & Schmidt 1994; see also Schlichenmaier et al. 1999). These theoretical models make use of the concept of penumbral flux tubes that act like convective bubbles carrying the energy upwards. In this model, the structuring of the penumbral magnetic field is directly related to the transport of energy by convection. A penumbral magnetic field structured in individual flux tubes is also used in the siphon flow models of Montesinos & Thomas 1997 (and references therein) to explain the Evershed effect (for a review see Thomas 1996; Solanki 1997). This paper discusses some of the spectroscopic signatures of the uncombed penumbral model proposed by Solanki & Montavon (1993, SM hereinafter) that partially accounts for this magnetic field structuring.

Observations have shown for decades a filamentary structure of the penumbra in continuum images (see, e.g., Sobotka 1997). The Evershed flow is also known to be highly structured, with flow channels extending radially in the penumbra. Title et al. (1993) and Rimmele (1995) concluded that the Evershed channels were well correlated with the dark penumbral fibrils seen in filtergrams. The filamentary condition of the penumbral magnetic field has been more difficult to investigate. Clear evidence of azimuthal fluctuations of the magnetic field inclination were found by Title et al. (1993) using magnetograms and by Degenhardt & Wiehr (1991) from Stokes V spectra. A similar conclusion was reached by Rimmele (1995). Data from the Advanced Stokes Polarimeter (ASP, see Skumanich et al. 1997) in the visible range showed that these inclination fluctuations were highly correlated with field strength fluctuations in the sense that vertical fields were stronger than horizontal ones (Lites et al. 1993, Stanchfield et al. 1997). Also using data from the ASP, but with a different analysis technique, Westendorp Plaza et al. (2000a, hereinafter WESa) found the same correlation between magnetic field strength and inclination. Martínez Pillet (1997) discussed the organization of penumbral magnetic fields into flux tubes with fluctuating inclinations and field strengths as well as their association with the Evershed flow. This connection between the Evershed flow and horizontal weak penumbral flux tubes has received additional support from recent infrared (IR) measurements. Rüedi et al. (1999) have used Ti I lines in the 2 μm region to find evidence for the existence of these concentrations. This work also shows how the low and horizontal field channels that carry the flow are associated with cooler temperatures (as shown by the strength of Ti I line), at least in the outer penumbral regions.

This better understanding of the penumbral magnetic field organization is incorporated in this paper into the model of SM and its predictions are compared with recent observational findings that are not yet fully understood. In particular, we scrutinize some of the results of the inversions carried out by WESa

and Westendorp Plaza et al. (2000b, hereinafter WESb, see also Fig. 1 in Westendorp Plaza et al., 1997). These authors find that almost everywhere in the outer penumbra (normalized radial distance larger than 0.7), the mean penumbral field strength increases with height (several hundreds of Gauss over the line-forming region) and that the field inclination decreases (over the same range) by as much as 30°. These conclusions are somewhat puzzling. First, any single-component model of a flux tube that opens up with height predicts a penumbral magnetic field that decreases upwards (see, e.g., Pizzo 1986). Second, and more important, it is impossible to account for a decrease of 30° in a range of heights of only 300 km (a typical line-forming region). That these inclination gradients are needed to explain the shapes of the circular polarization profiles observed in penumbrae is well known (Sánchez Almeida & Lites 1992; SM). The net circular polarization (NCP) observed in penumbrae (i.e., the integrated signal over the Stokes V profile) can only be satisfactorily explained with these large gradients (Sánchez Almeida & Lites 1992). But these gradients cannot be fitted into a single-component model of the penumbra (Solanki et al. 1993). Already Sánchez Almeida & Lites (1992) pointed out that the only way in which these gradients are realizable is as a result of the fine scale structure of the penumbra. The first model that explained the observed NCP taking into account the unresolved structured of the penumbral magnetic field was proposed by SM. In this model, horizontal tubes that carry most (but not all) of the Evershed flow, immersed in a more vertical background field, were able to predict the center-to-limb variation (CLV) of the observed NCP. This NCP was due to the fact that the line-of-sight (LOS) crossed the upper and lower boundaries of the horizontal tubes. The jumps in the field inclination seen by the LOS were of around 30° and, thus, were able to generate the NCP. The tube used by SM was of 150 km diameter which is large enough to cover an important fraction of a typical line forming region. But, as mentioned by SM, a set of many thinner piled up flux tubes will work as well. Indeed, Sánchez Almeida (1998) has proposed that the deduced $\approx 0.1^\circ/\mathrm{km}$ for the inclination gradient and the gradients derived from the $\nabla \cdot \boldsymbol{B} = 0$ condition applied to penumbral vector magnetic field data are only compatible with flux tubes with diameters of 1–15 km. These tubes are optically thin (for typical photospheric densities) and a large number of them are needed to generate the desired amount of NCP.

In this paper, we elaborate on SM model and introduce the above mentioned properties of the horizontal field channels (smaller field strength, lower temperatures; although hotter tubes are also considered for comparison). The NCP predicted from this model is then compared with recent ASP data (Sect. 2.1). We synthesize the Stokes spectra formed in this type of penumbral configuration and invert them with the SIR code (Ruiz Cobo & del Toro Iniesta 1992) to compare our results with the findings of WESa and WESb (including what they called "differential opacity effect", see Sect. 3). Similarly, we study how the SM model can be fine tuned to account for *all* the gradients as estimated from both, NCP and from the $\nabla \cdot \boldsymbol{B} = 0$ condition using one single flux tube. We also point out how this null divergence condition implies the existence of (reasonable) azimuthal magnetic fields.

2. The uncombed penumbral model

The penumbral magnetic field organization proposed by SM has one key ingredient. The two magnetic components proposed could not be separated in the vertical direction but rather the more vertical component winds around the horizontal flux tubes (that occupy a limited range of heights). This winding is responsible for the generation of the NCP in the model because the LOS will cross the boundaries between the two components. It is the jumps of the thermodynamic, magnetic and velocity parameters at the boundaries what generates the NCP. In the SM model, the jumps occupied a fixed optical depth interval of $\Delta \log \tau \approx 0.1$ simulating the effects of the two current sheets bounding the horizontal tubes. This optical depth interval corresponds approximately to 10–15 km in the atmosphere, which is of the order of a typical resistive boundary layer (Schüssler, 1986). In the uncombed penumbral model that we use, we preserve this key property of a more vertical component with field lines that flow past the horizontal flux tubes (the vertical component will be referred as the background component in the rest of the paper).

Our realization of the uncombed penumbral model is slightly different from that used by SM. The background model temperature is taken from the mean model derived by del Toro Iniesta et al. (1994). For reasons that will become clear later, we have scaled the temperature upwards by 5040/((5040/T)-0.01), which is equivalent to heat the atmosphere by 50 °K. After this scaling, the model is brought back to hydrostatic equilibrium (as it was the case of the original model). The background magnetic field strength we use follows the law: $1300 + 50 \log \tau$ in the optical depth interval $\log \tau = [-4, 1]$[1]. The inclination of the magnetic field is given by: $50 + \log \tau / 2$ over the same interval which implies a change of 2.5° over the whole atmosphere. This gives a net inclination gradient of $-0.0036^\circ/\mathrm{km}$ that fits very well in the interval allowed by Solanki et al. (1993). Micro- and macroturbulence are set everywhere equal to $1\,\mathrm{km\,s^{-1}}$. As it will be explained later, the macroscopic velocity in the background model could not be set to zero. To reproduce the CLV of the NCP an Evershed-like outflow of $1\,\mathrm{km\,s^{-1}}$ was used in the background model.

Following SM, the horizontal component is supposed to be organized into flux tubes that carry a larger part of the Evershed flow. Other properties of the horizontal tubes are different:

1. The tubes have a diameter of 100 km. Their height can be either 150 km above the $\tau_\mathrm{b} = 1$ level (the subscript b stands for the background model) or 250 km.
2. The horizontal tubes can be either cooler than the background or hotter (SM tubes were isothermal). The temperature profile of the tube is given by a gaussian with an amplitude of ± 500°K. The gaussian profile is used for

[1] all optical depths used in this paper refer to continuum optical depth at 5000 Å.

practical reasons in the treatment of the radiative transfer. Cooler tubes are suggested by the observations of Rüedi et al. (1999). On the other hand, the existence of hotter tubes is suggested by the simulations of Schlichenmaier et al. (1998): as part of the convective transport of energy, the rising tubes are hotter than their surrounding and optically thick. Once they reach the upper layers they radiate efficiently, cool down and become optically thin in the continuum. Thus both types of tubes (hot and cold) may play a role.

3. The magnetic field strength inside the tubes is always smaller than in the background model. The field strength profile in the tube follows the same gaussian as for the temperature. The amplitude of the gaussian is -500 G.
4. The gas pressure inside the tubes was forced to be in lateral equilibrium with the background total pressure: $p_{\rm b} + \frac{B_{\rm b}^2}{8\pi}$. This links the perturbation used in the tube field strength to the tube gas pressure and density (through the ideal gas law). The total optical thickness of the tube is then closely related to the perturbation used for the field strength. This was the reason to use a gaussian profile in the field strength instead of a step function. This latter case would have generated strong jumps in the optical thickness of the tube that could have been difficult to follow numerically.
5. The field inclination was not represented by a gaussian function but by a step function instead. As mentioned in the introduction, it is the jump in the field inclination what is known to be important for the generation of the NCP. The field inclination does not couple to any thermodynamic quantity and the jumps in this magnitude were much easier to treat numerically. The tubes were considered to have always a homogeneous field inclination of $\gamma_{\rm t} = 85^\circ$ (the subscript t stands for the tube model). The jump in inclination was then of around $\Delta\gamma \approx 35^\circ$.
6. The macroscopic velocity inside the tube was set to $2\,{\rm km\,s^{-1}}$. Note that this is only a factor two larger than that in the background model. This is similar to the velocities used by SM but contrast seriously with the simulations of Schlichenmaier et al. (1998).

The models are build on a geometrical height scale and afterwards their own optical depth scale is computed. Fig. 1 shows the stratifications of the background model (dotted lines) and of the model with a tube at a height of 150 km above the $\tau_{\rm b} = 1$ level. In the top left panel the temperature of the cold (solid) and hot (dashed) models are shown. The optical depth scale is very sensitive to the field strength perturbation (top right in the figure). Through the lateral total pressure balance condition, the density inside the tube increases by a factor 1.5 for the hot tube and by a factor 1.8 for the cold tube. The net effect, in both cases, is that the atmosphere below the tube has a higher optical depth than in the background and the local $\tau = 1$ is reached before. Because the $\tau = 1$ level is higher (at a smaller temperature), the continuum intensity is reduced for both hot and cold tubes. Thus, the temperature fluctuations that we are modeling correspond always to a darker structure compared to the background atmosphere. For models with tubes at 150 km above the $\tau_{\rm b} = 1$ level, the Wilson depression is 17 km. For tubes at 250 km, the Wilson depression is 9 km. The continuum intensity (normalized to the quiet sun) of the cold tube model at 150 km is 0.74 and 0.80 if the tube is at 250 km. For the hot tubes, the same numbers are 0.86 and 0.85 respectively. Because the background model had a slightly higher temperature than the original del Toro Iniesta et al. (1994) model, the continuum intensity of the background model is 0.93. Combining all these models with different filling factors one can obtain continuum intensities well within the observed range. Once the models have their own optical depth scale, the Stokes profiles of the Fe I lines at the 6302 Å region are synthesized using a Hermitian method to integrate the radiative transfer equation as proposed by Bellot Rubio et al. (1998). Unless stated otherwise, the profiles of the different models with horizontal tubes are always combined with the profiles derived from the background model using a filling factor of 50% for both atmospheres. In this way, we try to account for the unresolved nature of the penumbral fine structure.

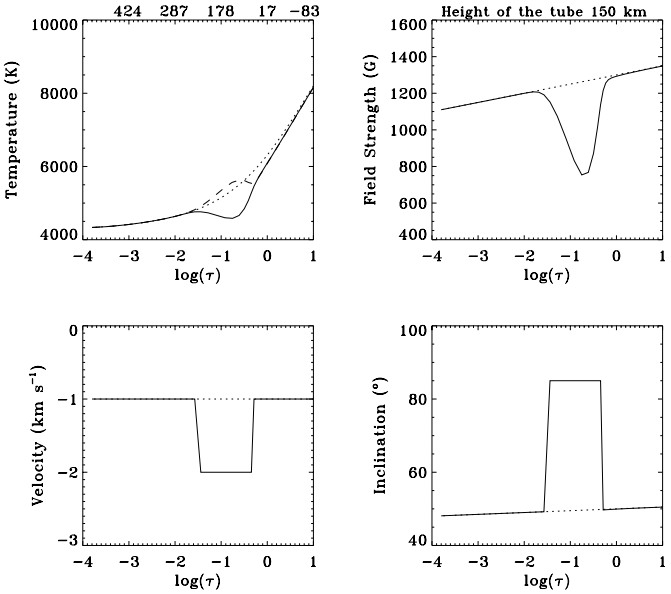

Fig. 1. From top left clockwise, temperature, field strength, magnetic field inclination and velocity of the background model (dotted lines) and of a modified model that includes a cold tube at a height of 150 km (solid lines). The dashed lines in the first plot represents the temperature run of a model with a hot tube. The numbers above this plot give the height (in km) from the $\tau_{\rm b} = 1$ level in the cold model.

The two bottom panels of Fig. 1 give the inclination with respect to the solar vertical of the background and tube model (right panel) and of the velocity (left panel). Note that this last case represent the modulus of the velocity in the models, not the disk center LOS values (that would be computed by multiplying this panel times the cosine of the inclination panel). The minus sign is used because the Evershed flow is an outflow and this is the sign convention used by SIR.

The models we have built have a number of ad-hoc properties. We do not claim that they perfectly represent the complex structuring of the magnetic field in penumbrae. We only expect

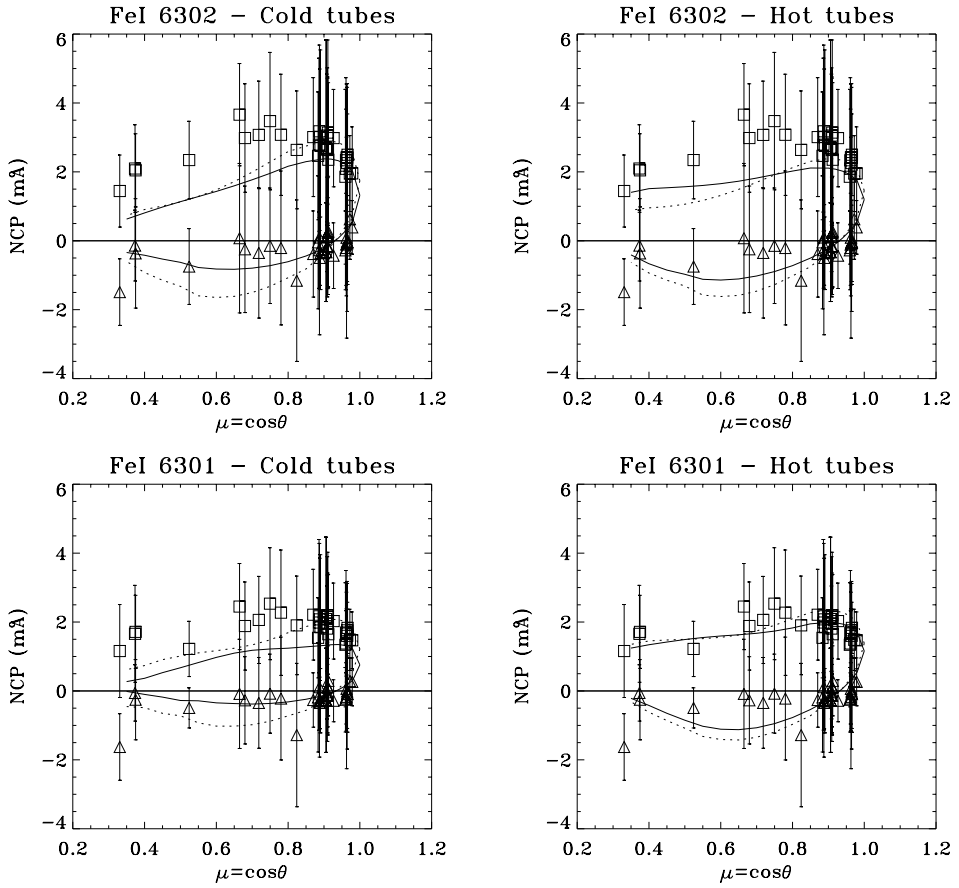

Fig. 2. Top left panel: CLV of the observed NCP for the Fe I line in the limb direction (squares) and in the center direction (triangles). The solid line is the prediction of the model with a cold tube at 150 km. Dashed line is for a cold tube at 250 km. Bottom left panel: The same but for Fe I 6301. Right panels correspond to tubes hotter than the environment.

from them to get an understanding of some of the recent observational results that simply do not fit with a smoother magnetic field representation.

2.1. CLV of the NCP derived from the model

SM already showed that the uncombed penumbral model predicts the observed NCP and its CLV in the center- and limb-side penumbra. However, it is important that we verify that our modified uncombed model still concurs with the observed NCP. We take advantage of new data of NCP derived from observations of the ASP. The observations are described in Martínez Pillet et al. (1997). Two sunspots within active regions NOAA 7197 and NOAA 7201 were followed during their disk passage. The two round leader sunspots of these active regions are used here to measure the NCP along the line that joins the disk center and the spot center. This line first passes through the so called center-side penumbra, crosses the umbra and leaves the spot passing through the limb-side penumbra. A four degree sector centered in the umbra is averaged to increase the number of points included in the statistics. Mean values and 3 times the standard deviation are plotted in Fig. 2 for the limb- (squares) and center-side penumbra (triangles) as a function of the cosine of the heliocentric angle $\mu = \cos\theta$. The upper panels of Fig. 2 correspond to Fe I line at 6302.5 Å and the bottom panels to Fe I line at 6301.5 Å. The predictions of the uncombed model for cold and hot tubes (left and right respectively in Fig. 2) and for tubes at 150 km and at 250 km above $\tau_{\rm b} = 1$ (solid and dotted lines respectively) are shown. (In all cases a filling factor of 50% has been assigned to both the background model and the model with the horizontal tubes.) Several well known features can be recognized. The limb-side penumbra has a larger NCP, and of opposite sign, to that in the center-side penumbra. However, note that for $\mu > 0.96$ the mean values of the NCP in the center-side penumbra do have a tendency to be of the *same* sign as in the limb-side penumbra. This fact has not been clearly acknowledged in previous observational works, something that may be due to the lower spatial resolution of the data used (the best resolution of our ASP data is somewhere between 1–2 ″). Our CLV curves predict that a penumbra observed right at disk center will show an NCP of 1.15 mÅ for Fe I 6301.5 Å and of 1.49 mÅ for Fe I 6302.5 Å.

The error bars in Fig. 2 give an idea of the range of observed values. We do not expect to generate a good fit to these data with our realizations of the uncombed penumbral model. But, rather, we expect the predictions of the models to fall somewhere within the observed range. Note that these predictions do not include an average of the penumbral conditions at different radial distances (i.e. like averaging different inclinations of the background model) but they refer to one single radial point somewhere in the outer penumbra. Taking this into account and considering that no parameter search has been made, the agreement is quite satisfactory.

The models clearly show the (observed) rapid fall towards negative values of the center-side penumbra NCP at high μ values, including an NCP=0 crossing point. This zero NCP point does not depend on the height of the tube. It is easy to understand why the uncombed penumbral model has a point in the center-side penumbra where no NCP is generated. As pointed out by SM, wherever the LOS velocities of the background and tube models are the same, no NCP is generated. This implies solving the equation $v_{\rm t}\cos(\gamma_{\rm t}\pm\theta) = v_{\rm b}\cos(\gamma_{\rm b}\pm\theta)$ where the $+$ sign applies to the limb-side and the $-$ to the center-side penumbra. In our case, $v_{\rm t} = -2$ kms^{-1}, $v_{\rm b} = -1$ kms^{-1}, $\gamma_{\rm t} = 85^\circ$ and $\gamma_{\rm b}\approx 50^\circ$ gives a solution only for the center-side penumbra at a μ value of 0.93. These considerations also show that the CLV of the NCP makes very difficult an scenario where the background velocity would be zero ($v_{\rm b} = 0$ kms^{-1}). In this case, the NCP=0 point would be seen in the limb-side penumbra (as long as $\gamma_{\rm t} < 90^\circ$). Thus, if the flux tubes are close to the horizontal, but not diving down within the penumbra, the Evershed outflow should also be present in the background model.

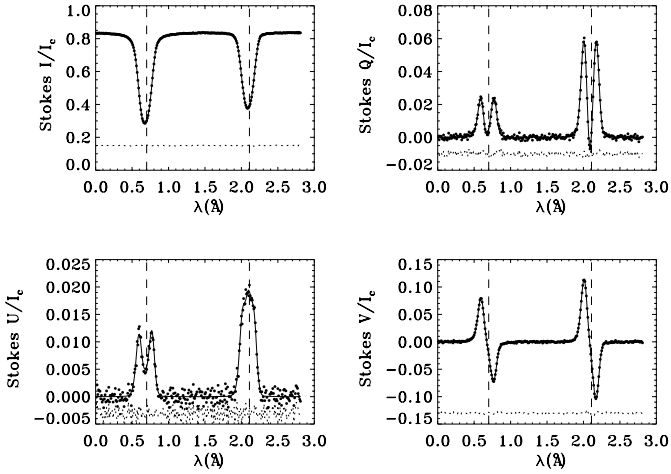

Fig. 3. Stokes parameters for the Fe I 6301 and 6302 lines in the cold model with tubes at 150 km height. A filling factor of 50% is assumed for this model, the rest being the background model. Dots: synthetic data, solid lines: fit produced by SIR, dotted lines: residuals. Vertical dashed lines: rest wavelengths.

3. Results from the inversion code

In this section, we study if our modified uncombed model can explain some of the results obtained by WESa,b. In particular, we expect the horizontal flux tubes included in the model to be misinterpreted by the SIR inversion code as long as they remain unresolved. The SIR code has been thoroughly tested in the past (Ruiz Cobo & del Toro Iniesta, 1992; Westendorp Plaza et al., 1998). These last authors also retrieved successfully atmospheric models that included sharp discontinuities along the LOS (canopy-like atmospheres). But all these tests refer to homogeneous atmospheres. That is, they simulate observations where all LOS contributing to the observed profiles pass through the same atmosphere. With 1 $''$, or worse, resolution, it is clear that the structure of the penumbral magnetic field remains unresolved and that the observed profiles are coming from a combination of profiles formed in very different atmospheric conditions. We believe this is at the origin of the increase of the penumbral field strength and the sharp decrease of the inclination deduced by Westendorp Plaza and co-workers.

To prove this point, the profiles built in Sect. 2 (at disk center and with a filling factor of 0.5 for the background and tube models) are introduced as simulated observations into the SIR code. The synthetic profiles have noise added to simulate a S/N of 10^3 (similar to the ASP). The initial guess model is the background model and the number of nodes[2] used is similar to those in WESa,b. In Fig 3, we show the synthetic profiles (dots) and the fit produced by SIR (solid lines). The fit is as good as it can be for this S/N level (see the residual in the Stokes U panel). The blueshift (rest wavelength is given by the vertical dashed lines) produced by the Evershed outflow is evident in all Stokes profiles. The Stokes V profile coming from the model with the tube has an NCP of 1.6 mÅ and 2.9 mÅ for the Fe I 6301 and 6302 lines respectively. The profiles in Fig. 3 have around half these values because the background profiles are almost perfectly antisymmetric.

The interesting result here is the atmospheric model retrieved by SIR. It is shown in the four panels of Fig. 4 with dotted lines and error bars. The output SIR model is compared with a "mean" atmospheric model made after averaging the tube model and the background model (solid line). This average is first made in a geometrical height scale and afterwards its own optical depth scale is computed. Note that this model does not correspond to the model of any particular point in the atmosphere, it only represents average conditions within the resolution element that produced the synthetic profiles input to SIR. As can be seen in the right panels, the field strength (top) increases with height (around 600 G in the range $\log\tau = [-3, 0]$) and the field inclination (bottom) decreases abruptly from 74° to less than 40° at the top of the atmosphere. Thus, the synthetic profiles produced by the (unresolved) uncombed model are interpreted by SIR in a way that *resembles* very much the results of WESa,b. The SIR code only feels the effect of the tubes at the deeper layers and it fixes the atmospheric gradients accordingly. But it never retrieves the localized perturbation. This result also applied to the profiles coming from hot tubes and from tubes at a height of 250 km above the $\tau_{\rm b} = 1$ level. We want to emphasize that this deceptive looking fit is not a fault of the SIR code. But rather, it represents the failure of one of the assumptions: that the atmosphere that generates the profiles is homogeneous. If we feed SIR with profiles generated from the tubes models but mixing no background contribution (i.e., a filling factor of one or, equivalently, a resolved uncombed penumbral model), SIR does a much better job in reproducing the perturbation represented by the tubes. Indeed, in the top part of the Field Strength panel of Fig. 4, we show the fit (thin dashed line, shifted upwards by 1500 G) produced when the filling factor is one. The

[2] the nodes in SIR are the optical depth points where the perturbations of the atmospheric parameters are computed to generate a new model that provides a better fit.

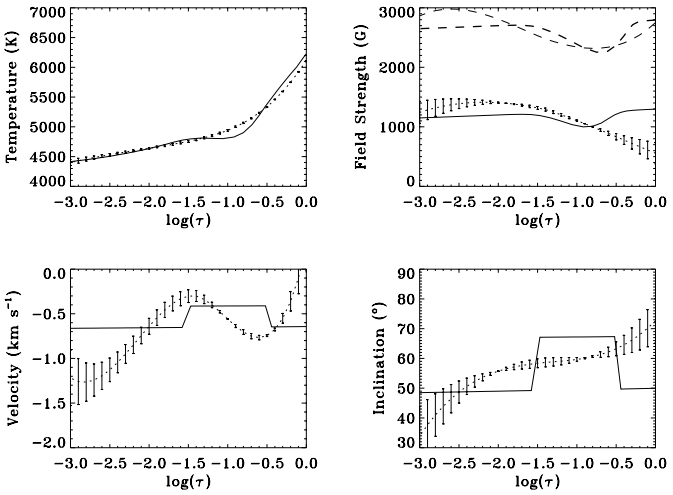

Fig. 4. Atmospheric models resulting from the inversion of the profiles in Fig. 3. Dotted lines: model derived by SIR and error bars. Solid line: model produced from averaging 50% of the model with a cold tube and 50% of the background model. See text for details.

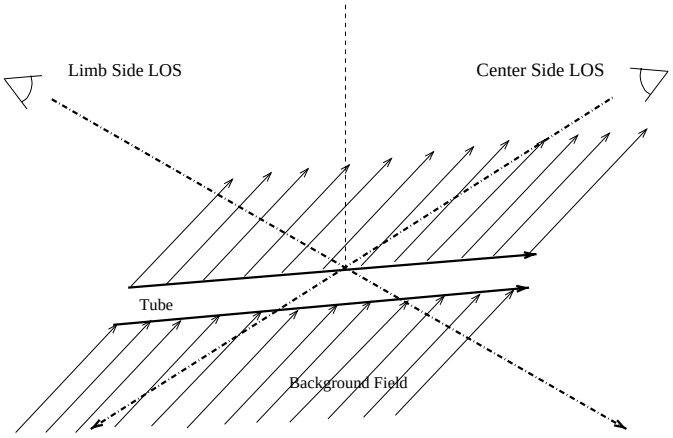

Fig. 5. Representation of the path of a limb-side LOS and a center-side LOS. Both lines cross the penumbral background field and the penumbral flux tube but the cross-section of the tube seen by the center-side LOS is larger than for the limb-side LOS. The dashed line represents the solar vertical.

thick dashed line is the same as in Fig. 1, also shifted by 1500 G.

WESa,b detected in their inversions what they called a "differential opacity effect" between the limb- and center-side penumbra. The reason to invoke a differential opacity was the fact that at $\log\tau = 0$ in the limb-side penumbra, SIR retrieved field vectors at 90° (or slightly larger) and redshifted LOS velocities while, at the center-side penumbra, smaller inclinations and blueshifted LOS velocities were found. Here, we investigate the origin of the differential opacity effect in the framework of the uncombed model. That, in general, one would probe different geometrical heights (for the same optical depths) in the limb- and center-side penumbra is easily seen from Fig. 5. The center- and limb-side LOS "see" a very similar atmosphere until they reach the top part of the tube. From there on, the path

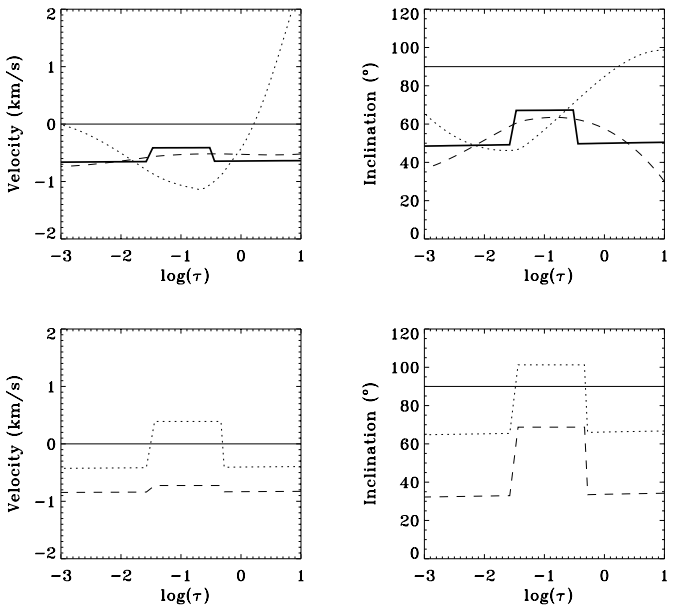

Fig. 6. Top left: LOS Velocity as retrieved from SIR for the limb- (dotted) and center-side (dashed) penumbra. The models are projected so that the abcisae are measured along the local vertical. Thick solid line gives the mean stratification. Top right: The same but for Inclination. Bottom left: projected velocities along the LOS for the limb- (dotted) and center-side (dashed) penumbrae. Bottom right: Inclination projected along the LOS for the two cases.

they follow inside it is different for each LOS. The limb-side LOS transverses a total length of $d/\sin(\gamma_t + \theta)$ (d being the width of the tube). On the other hand, the center-side LOS has a larger path within the structure $d/\sin(\gamma_t - \theta)$. The tubes have a higher density than the background model and these different paths introduce a net difference in the optical depths seen at the two penumbral sides. In our case $\gamma_t = 85°$ and for the sunspot analyzed by WESa,b $\theta = 15.6°$, the difference in the paths between the limb- and center-side penumbrae is only of around 5%, which is too small to explain the observed differences. A more significant path difference of 20% or larger is achieved for $\mu < 0.6$. So, our realization of the uncombed penumbral model does not seem to generate a big enough differential opacity effect (we have quantified this to be of only a few kilometers). Note, however, that this result is very sensitive to the actual value of γ_t. If this value is smaller than the one we use (as the footpoints of the elevated Evershed channels of Rimmele 1995 would indicate) the effect can be more pronounced.

In order to understand, then, the differences observed by WESa,b, we have used our profiles synthesized at $\mu = 0.96$ in the center- and limb-side penumbra and analyzed them with SIR. In what follows, we refer only to the model with cold tubes at a height of 150 km. The actual profiles that were inverted had a 0.5 filling factor of background model added and noise to simulate a S/N of 10^3. The results are seen in Fig. 6. The top panels are the stratifications retrieved by SIR for the velocity (left) and magnetic field inclination (right). These figures display atmospheric models corrected for projection effects. That

is, they provide the atmospheric quantities as they would be seen by an observer looking straight down into the penumbra. The limb-side stratifications (dotted lines) show the same qualitative effects as obtained by Westendorp Plaza and coworkers. In the layers around $\log\tau = 0$ one finds redshifted velocities and inclinations that are close to 90°. This is not observed in the center-side results (dashed lines). Both models are much more similar at layers around $\log\tau = -1.5$ in agreement with WESa,b. The average stratification (50% tube model, 50% background) is given in both cases by the thick solid line. As stated before, this difference cannot be understood in terms of observing different geometrical heights in each side of the penumbra. We believe the reason for these differences to be in the actual difference between the profiles synthesized in each penumbral side and the analysis carried out by SIR. In the bottom panels of Fig. 6, we plot the stratifications along the LOS that generated the profiles at the limb- (dotted) and center-sides (dashed). The LOS velocity at the limb-side shows a very strong gradient at the tube location which generates profiles that do not preserve the usual symmetry properties of the Stokes parameters (Q and U symmetric and V antisymmetric). Indeed, because of the large velocity gradient and the polarity change in the magnetic field inclination, the Stokes V profile coming from the tube atmosphere shows the well-known "cross-over effect" (Grigorjev & Katz 1972, 1975; but note that the background model does not). However, the LOS velocity in the center-side penumbra shows a very small velocity gradient (dashed line) and the tube profiles are almost perfectly symmetric (antisymmetric for Stokes V). This agrees with the fact that the center-side penumbral model at this μ value shows negligible NCP (see Fig. 2). The difference between the symmetries of the profiles at these two sides and the gradients needed by SIR to reproduce them explains the contrast between the results obtained at each penumbral side.

4. Gradients from the model

In a recent paper, Sánchez Almeida (1998) has proposed that the existing estimates of the inclination gradient are only compatible with penumbral magnetic structures with sizes in the range of 1 to 15 km. The estimates used there correspond to the quantity:

$$P = \frac{\partial \cos\gamma}{\partial z}, \qquad (1)$$

where z indicates height in the atmosphere. Values of $\langle P\rangle$ ($\langle\rangle$ means some kind of average over the resolution element volume) and its rms fluctuations can be obtained from different sources. For example, from a sunspot vector magnetogram one can use $\langle B_x\rangle$, $\langle B_y\rangle$ and $\langle B_z\rangle$ together with the $\nabla\cdot\boldsymbol{B} = 0$ and infer mean values of $P = 1/B(\partial B_z/\partial z)$, (following Sánchez Almeida 1998, we neglect in this section variations of B with height) and the rms fluctuations between different pixels ($\langle P\rangle_{rms}$). An estimate of a quadratic mean ($\langle P^2\rangle^{1/2}$) can be obtained from the measurements of NCP (that is assumed to provide a similar volume average as before). This is a much less direct estimate than the mean of $\langle P\rangle$, but Sánchez Almeida (1998) shows that, under some assumptions, one can expect a proportionality between $\langle P^2\rangle$ and the measured NCP. The estimates found in this way are given in the first row of Table 1.

Table 1. Inclination gradients

Source	$\lvert\langle P\rangle\rvert$ (km^{-1})	$\langle P^2\rangle^{1/2}$ (km^{-1})	$\langle P\rangle_{rms}$ (km^{-1})
Observations[a]	2.0 10^{-5}	3.0 10^{-3}	1.0 10^{-4}
150 km 100%	4.7 10^{-5}	3.0 10^{-3}	
150 km 50%	4.7 10^{-5}	1.0 10^{-3}	
250 km 100%	4.7 10^{-5}	3.0 10^{-3}	
250 km 50%	4.7 10^{-5}	1.0 10^{-3}	
random z_t model			2.8 10^{-4}

[a] From Sánchez Almeida (1998)

Using the models built here, we can estimate the magnitude of these different average gradients. The $\langle P\rangle$ is easily measured from the models as the average with height of the quantity defined by Eq. (1). It is important here to point out that, in the uncombed model, $P(z)$ is a function that has two sharp peaks of opposite signs. The location of the peaks corresponds to the bottom (negative peak) and the top of the tube (positive peak). These two jumps cancel in the final $\langle P\rangle$ if they are equally weighted by the averaging process. Thus, $\langle P\rangle$ is determined from the gradient of the background model. In Table 1, we give (first column) the value of $\langle P\rangle$ for the models with tubes at 150 km and 100% filling factor (second row), 150 km and 50% filling factor (third row), 250 km and 100% filling factor (fourth row) and 250 km with 50% filling factor (fifth row). In a similar way, one trivially computes $\langle P^2\rangle^{1/2}$ as predicted by these models (second column of Table 1). But now, when one computes the quadratic mean of P, the two jumps *do not* cancel. Indeed, it is the magnitude of the jumps at the tube boundaries, and the fraction of heights that they occupy, that determines the value of $\langle P^2\rangle^{1/2}$. In this case, the contribution of the background gradient is negligible. Interestingly, the linear and quadratic averages in Table 1 agree very well with the observed ones. The almost two orders of magnitude difference between them are naturally explained from the fact that, in the first case (linear mean), the contributions of the boundaries of the tubes cancel while, in the second case (quadratic mean), they do not. The almost perfect match between the models and the observations should be no mystery. It is due to selecting as inclination jump (30°) the value needed to explain the NCP (which in turn determines $\langle P^2\rangle^{1/2}$; see Sánchez Almeida & Lites, 1992; SM; Sánchez Almeida, 1998).

We note in passing that our study also supports a proportionality between the NCP and the value of $\langle P^2\rangle$ (Sánchez Almeida, 1998). In particular, although the agreement between the magnetic field inclination of the average atmosphere and the atmosphere retrieved by SIR in the bottom right panel of Fig. 4 is not particularly good, both models share the *same* value of $\langle P^2\rangle$ (but a totally different value of $\langle P\rangle$). Because both models generate Stokes V profiles with the same NCP, a proportionality seems to hold between these two magnitudes.

The estimate of $\langle P\rangle_{rms}$ cannot come directly from our four uncombed penumbral models. To obtain a sensible estimate of this quantity, we need to say something about how different realizations of the model can display different values of $\langle P\rangle$. To this end, we follow a scheme where the different realizations correspond to random values of the tube height within the line forming region (Sánchez Almeida, private communication). A penumbral flux tube centered at a height z_t will contribute with a mean gradient of:

$$\langle P\rangle(z_t) = \int_{-\infty}^{+\infty} P(z, z_t) g(z)\, dz. \quad (2)$$

Here, the function $g(z)$ represents a weighting function assigned to each atmospheric height z. For the order-of-magnitude estimate we pursue, a gaussian representation of g representing a typical line forming region will suffice. $P(z, z_t)$ is the gradient as estimated from Eq. 1 when the tube is at z_t. To estimate the rms fluctuations, we assume that the random variable z_t has a flat density distribution in the range [-100,400] km. That is, there will always be one tube centered somewhere in this range, all heights being equally probable. $P(z, z_t)$ has contributions from the tube and from the background atmosphere. The latter, being always the same, does not contribute to the rms values. Here, we use a constant background inclination with a null contribution to P. To compute Eq. 2, we further assume that the tubes remain the same as they travel through the atmosphere (that is, for different values of z_t). This invariance allows us to treat Eq. 2 as the convolution of the two functions g and P. For $g(z)$, we use a unit area gaussian with a FWHM of 200 km (shown in Fig. 7). $P(z, z_t)$ is taken as the combination of two gaussians of opposite sign separated by 100 km (the tube size) and, both, with a FWHM of 10 km (also shown in Fig. 7). Note that, now, the amplitude of the gaussians is given by the fact that their integral should account for the total jump in inclination: $\Delta \cos\theta = \cos(55^\circ) - \cos(85^\circ)$. The convolution of these two functions, $\langle P\rangle(z_t)$, is shown in Fig. 7 with a dashed line. This function can be used to estimate the rms values of fully resolved penumbral observations. These observations would correspond to independent realizations of the model for random choices of the tube height z_t. According to Fig. 7, the peak to peak variation of these realizations would be 0.0026 km^{-1} and the resulting rms would be three times smaller, 8.7 10^{-4} km^{-1}. Now, if we take into account that the observations in Table 1 have a spatial resolution of around 1000 km, we should reduce this rms by an additional factor of $\sqrt{10}$. The exact value is given in the last row of Table 1 as our rms estimate. Given all the simplifications made in this calculation, the agreement between our estimate ($\sim$3 10^{-4} km^{-1}) and the observed value (1 10^{-4} km^{-1}) is more than satisfactory. The quadratic mean predicted in this random z_t model also compares satisfactorily with the observed value.

We, then, conclude that even if the observed values of $\langle P^2\rangle^{1/2}$ and $\langle P\rangle$ differ by almost two orders of magnitude, the uncombed penumbral model proposed by SM is able to predict this difference. Building a range of $\langle P\rangle$ values that gives rise to the observed rms fluctuations seems not to be a problem for the model as well. However, one may question how can penumbrae have locally mean values of $P(z)$ as large as several 10^{-2} km^{-1} while, at the same time, preserving the $\nabla \cdot \boldsymbol{B} = 0$ condition. Remember that this value is one order of magnitude larger than $\langle P^2\rangle^{1/2}$ and three orders of magnitude larger than the observed $\langle P\rangle$ (which is derived from using the $\nabla \cdot \boldsymbol{B} = 0$ averaged over the resolution element). To study the implications of these large local values of $P(z)$, we write the null divergence condition in cylindrical coordinates in the following form:

$$\frac{\partial B_\phi}{\partial \phi} = -r \frac{\partial B_z}{\partial z} = -rBP(z), \quad (3)$$

where we have neglected the contribution of the radial term (this is perfectly justifiable in the mid penumbra). Eq. (3) tells us that the local jumps in $P(z)$ should be accompanied by newly generated azimuthal fields B_ϕ. This is nothing but stating that the background field lines cannot end where they find the tubes, but have to wind around them. How large are these azimuthal fields? If we re-write Eq. (3) as:

$$|B_\phi| = r\Delta\phi BP(z) \approx \frac{BP(z)d}{2}, \quad (4)$$

(with d the tube diameter) we estimate the magnitude of the azimuthal field to be $B_\phi \approx B$, i.e., a purely azimuthal field vector.

Already SM, noticed the need for these azimuthal fields, although they did not estimate their importance. SM pointed out that the azimuthal fields needed at the top and at the bottom of the tubes give a contribution of opposite sign to the NCP and, thus, they were neglected in the radiative transfer (as we have done here).

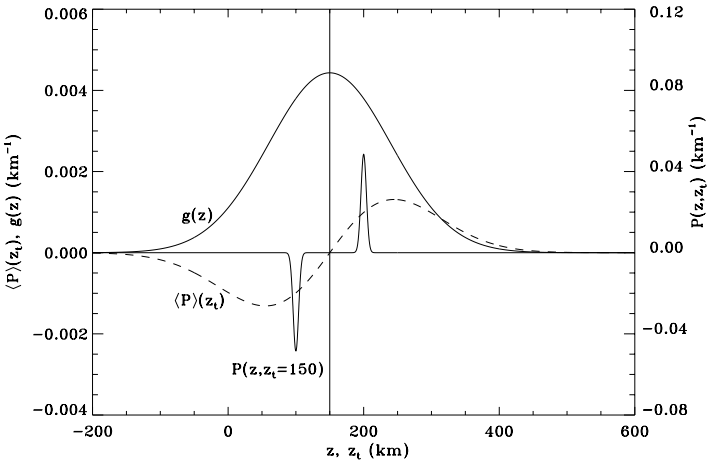

Fig. 7. Inclination gradient ($P(z)$, solid line, right ordinate), weighting function ($g(z)$, solid line, left ordinate) and the convolution of these two functions ($\langle P\rangle(z_t)$, dashed line, left ordinate) as a function of height in the atmosphere ($P(z)$ and $g(z)$) or as a function of penumbral flux tube height ($\langle P\rangle(z_t)$). The vertical line corresponds to the maximum of the weighting function.

5. Conclusions

The uncombed penumbral model proposed by Solanki & Montavon (1993) provides a satisfactory framework to understand

recent observational results. The inversions of Westendorp Plaza and co-workers nicely fit in the description of the unresolved structure of the penumbral magnetic field proposed by the uncombed model. Similarly, the model easily predicts the linear, quadratic and rms gradients analyzed by Sánchez Almeida (1998). This is possible thanks to the rather peculiar statistics of P generated in the uncombed model. This statistics is dominated by three possible values of the gradient, a very small P over most of the atmosphere and orders-of-magnitude larger P at the tube boundaries that can be either positive or negative. But we have to bear in mind that a description of the penumbral magnetic field in terms of horizontal flux tubes with smaller field strengths and a background magnetic field can only be a first order description of a real penumbra. A generalization of this model would include a highly structured magnetic field with probably no "background field". All field lines would be part of penumbral tubes that are participating in the convective process that makes penumbrae so bright (in spite of having field strengths that are only a factor 2 smaller than umbrae). This generalization can provide a natural way to explain one of the less satisfactory results of the uncombed model. We are referring to the fact that a model where one would concentrate all Evershed flow in the horizontal tubes but put no flow in the background field (as used in Schlichenmaier et al. 1998 simulations) is totally incompatible with observations. If this were the case, the center- and limb-side NCP curves would be almost the same but with different signs (as already pointed out by SM). This is in severe contrast with the observations. The difference between these two penumbral sides can only be explained by using a background field that carries a smaller (but significant) part of the Evershed flow. In our opinion, the results of this paper are showing nothing but what would be the signs of the correlations that a more elaborated uncombed model would have. For example, if those tubes that are rising (as part of the convective process) suffer a deceleration of the outward flow when they reach the upper part of the spectral line forming layer, a net effect like the one we have modeled will result. Similarly, one can think of descending tubes that suffer an acceleration of the outward flow. Evidence for hot rising and cold sinking plasma elements has been reported recently by Schlichenmaier & Schmidt (1999). Thus, a better understanding of how energy is transported in the presence of a horizontal field and the resulting magnetic field structuring is strongly needed. It is interesting to point out that at present spectroscopic resolutions (1 $''$) one can have, in the volume contributing to the observations, more than 20 tubes similar to those modeled here (we have used, in our volume, only around 5 of them).

From an observational point of view, a natural next step should be an analysis of the predictions of the uncombed model by using inversion techniques. The SIR code can be complemented with a physical scenario that accounts for the unresolved nature of the penumbral structure. This scenario can be, as a first step, an uncombed model with one tube and a background field. By least-square fitting of the observed profiles, one would obtain a great deal of information that in this work has been prescribed ad-hoc. Although, as we have stated before, a model with one tube and a background field may not be realistic, it would provide useful information about the correlations that prevail in the penumbrae of sunspots.

Acknowledgements. Help with the SIR code by Dr. L. Bellot Rubio and Dr. B. Ruiz Cobo is gratefully acknowledged. Dr. J.C. del Toro Iniesta carefully read the manuscript. Criticism by Dr. J. Sánchez Almeida on a previous estimate of the rms gradients is acknowledged. The ASP data used in this work is part of a collaboration with Dr. B.W. Lites and Dr. A. Skumanich from HAO/NCAR. This project was partly funded by the Spanish DGYCIT under project 95-0028-C.

References

Bellot Rubio L., Ruiz Cobo B., Collados M., 1998, ApJ 506, 805
Degenhardt D., Wiehr E., 1991, A&A 252, 821
del Toro Iniesta J.C., Tarbell T.D., Ruiz Cobo B., 1994, ApJ 436, 400
Grigorjev V.M., Katz J.M., 1972, Sol. Phys. 22, 119
Grigorjev V.M., Katz J.M., 1975, Sol. Phys. 42, 21
Jahn K., Schmidt H.U., 1994, A&A 290, 295
Lites B.W., Elmore D.F., Seagraves P., et al., 1993, ApJ 418, 928
Martínez Pillet V., 1997, In: Schmieder B., del Toro Iniesta J.C., Vázquez M. (eds.) Advances in the physics of sunspots. ASP Conf. Ser. vol. 118, p. 212
Martínez Pillet V., Lites B.W., Skumancih A., 1997, ApJ 474, 810
Montesinos B., Thomas J.H., 1997, Nat 390, 485
Pizzo V.J., 1986, ApJ 302, 785
Rimmele T.R., 1995, A&A 298, 260
Rüedi I., Solanki S.K., Keller C.U., 1999, A&A 348, L37
Ruiz Cobo B., del Toro Iniesta J.C., 1992, ApJ 398, 375
Sánchez Almeida J., 1998, ApJ 497, 967
Sánchez Almeida J., Lites B.W., 1992, ApJ 398, 374
Schlichenmaier R., Schmidt W., 1999, A&A 349, L37
Schlichenmaier R., Jahn K., Schmidt H.U., 1998, A&A 337, 897
Schlichenmaier R., Bruls J.H.M.J., Schüssler M., 1999, A&A 349, 961
Schmidt H.U., 1991, Geophys. Astrophys. Fluid Dyn. 62, 249
Schüssler M., 1986, In: Deinzer W., Knölker M., Voigt H.H. (eds.) Small scale magnetic flux concentrations in the solar photosphere. Göttingen, p. 103
Skumanich A., Lites B.W., Martínez Pillet V., et al., 1997, ApJS 110, 357
Sobotka M., 1997, In: Schmieder B., del Toro Iniesta J.C., Vázquez M. (eds.) Advances in the physics of sunspots. ASP Conf. Ser. vol. 118, p. 155
Solanki S.K., 1997, In: Alissandrakis C.E., et al. (eds.) Solar and Heliospheric Plasma Physics. Springer, p. 49
Solanki S.K., Montavon C.A.P., 1993, A&A 275, 283 (SM)
Solanki S.K., Walther U., Livingston W., 1993, A&A 277, 639
Stanchfield II D.C.H., Thomas J.H., Lites B.W., 1997, ApJ 477, 485
Thomas J.H., 1996, In: Flows K.C., Tsinganos (eds.) Solar and Astrophysical Magnetohydrodynamic. Kluwer, p. 39
Title A.M., Frank Z.A., Shine R.A., et al., 1993, ApJ 403, 780
Westendorp Plaza C., del Toro Iniesta J.C., Ruiz Cobo B., et al., 1997, In: Schmieder B., del Toro Iniesta J.C., Vázquez M. (eds.) Advances in the physics of sunspots. ASP Conf. Ser. vol. 118, p. 202
Westendorp Plaza C., del Toro Iniesta J.C., Ruiz Cobo B., et al., 1998, ApJ 494, 453
Westendorp Plaza C., del Toro Iniesta J.C., Ruiz Cobo B., et al., 2000a, ApJ in press, WESa
Westendorp Plaza C., del Toro Iniesta J.C., Ruiz Cobo B., et al., 2000b, ApJ in press, WESb